Nonlinear Localization of Dissipative Modulation Instability

Alexander U. Nielsen,[1,2] Yiqing Xu,[1,2] Caleb Todd,[1,2] Michel Ferré,[3] Marcel G. Clerc,[3] Stéphane Coen,[1,2] Stuart G. Murdoch,[1,2] and Miro Erkintalo[1,2,*]

[1]*The Dodd-Walls Centre for Photonic and Quantum Technologies, New Zealand*
[2]*Physics Department, The University of Auckland, Private Bag 92019, Auckland 1142, New Zealand*
[3]*Departamento de Física and Millenium Institute for Research in Optics, Facultad de Ciencias Físicas y Matemáticas, Universidad de Chile, Casilla 487-3, Santiago, Chile*

(Received 18 April 2021; accepted 12 August 2021; published 15 September 2021)

Modulation instability (MI) in the presence of noise typically leads to an irreversible and complete disintegration of a plane wave background. Here we report on experiments performed in a coherently driven nonlinear optical resonator that demonstrate nonlinear localization of dissipative MI: formation of persisting domains of MI-driven spatiotemporal chaos surrounded by a stable quasi-plane-wave background. The persisting localization ensues from a combination of bistability and complex spatiotemporal nonlinear dynamics that together permit a locally induced domain of MI to be pinned by a shallow modulation on the plane wave background. We further show that the localized domains of spatiotemporal chaos can be individually addressed—turned on and off at will—and we explore their transport behavior as the strength of the pinning is controlled. Our results reveal new fundamental dynamics at the interface of front dynamics and MI, and offer a route for tailored patterns of noiselike bursts of light.

DOI: 10.1103/PhysRevLett.127.123901

Modulation instability (MI) is a universal process that manifests itself in countless conservative and dissipative physical systems [1–5], describing the instability of a plane wave background to periodic perturbations. It is among the most celebrated processes in nonlinear science, fundamentally linked to the formation of patterns [6–8], solitons [9–13], and rogue waves [14–18]. MI is also central to key technological applications, including fiber supercontinuum generation [19] and microresonator optical frequency combs [20–22].

MI is typically examined via linear stability analyses that consider the evolution of low-amplitude periodic perturbations on a plane wave background. Recently, however, there has been considerable interest in exploring MI dynamics in the presence of strong localized perturbations that trigger directly the nonlinear stages of MI [23–29]. These studies reveal the formation of an expanding domain of spatiotemporal complexity—surrounded by the residual plane wave background—whose fronts propagate at quasiconstant velocity [25–32]. An interesting question that arises is: can the propagation of the fronts be arrested, and the complexity born from MI consequently be confined within a finite domain *ad infinitum*? For systems that have been extensively studied to date—such as those modeled by the conservative nonlinear Schrödinger equation (NLSE)—the answer appears to be no. This is because unavoidable broadband noise present in any real (laboratory) setting will ultimately cause the plane wave background surrounding the domain to undergo spontaneous MI. Indeed, sustainment of persisting domains requires bistability between a stable plane wave state and a spatiotemporally complex state born from MI [33,34].

Here we experimentally demonstrate controlled nonlinear localization of MI in a bistable system that has attracted significant recent attention in its own right [13,20–22,30,31,35]—a coherently driven Kerr nonlinear optical ring resonator. Specifically, we show that a shallow modulation applied to the amplitude of the coherent driving field can pin the fronts of a locally induced domain of MI-driven spatiotemporal chaos [30,31], permitting persistent nonlinear localization despite the fact that at all points the driving exceeds MI threshold. Moreover, we show that the domains can be individually addressed—turned on and off at will—and we explore their transport behavior as the strength of the pinning is controlled. Our results extend experimental studies pertaining to the nonlinear stages of MI [29] into dissipative systems [36], and could pave the way for novel sources of laser light that produce customizable patterns of noiselike bursts of light [37,38].

We first describe the nonlinear dynamics that underpin our experiments. The coherently driven resonator system pertinent to our study is modeled by the damped-driven NLSE, which in dimensionless form reads [7,21,36,39]

$$\frac{\partial\psi(t,\tau)}{\partial t} = \left[-1 + i(|\psi|^2 - \Delta) + i\frac{\partial^2}{\partial\tau^2}\right]\psi + \sqrt{X}. \quad (1)$$

Here $\psi(t,\tau)$ describes the slowly varying electric field envelope inside the resonator, t is a "slow" time variable that describes the evolution of $\psi(t,\tau)$ over consecutive

round-trips, and τ is a spacelike variable that describes the envelope's profile over a single round-trip. The terms on the right-hand side of Eq. (1) respectively describe dissipation, Kerr nonlinearity, frequency detuning of the driving field from a cavity resonance (Δ is the detuning parameter), (anomalous) group-velocity dispersion, and coherent driving (X is the driving intensity). We note that the presence of dissipation and driving renders Eq. (1) fundamentally different from the conservative NLSE [40].

Localization of MI (as defined in the context of this paper) requires coexistence between a stable plane wave state and a spatiotemporally chaotic state born from MI that can persist *ad infinitum* [33,34]. The system described by Eq. (1) provides such coexistence for detunings $\Delta \gtrsim 4$ [30,32]. In this regime, the homogeneous steady-state solutions of Eq. (1) display an S-shape characteristic of bistability

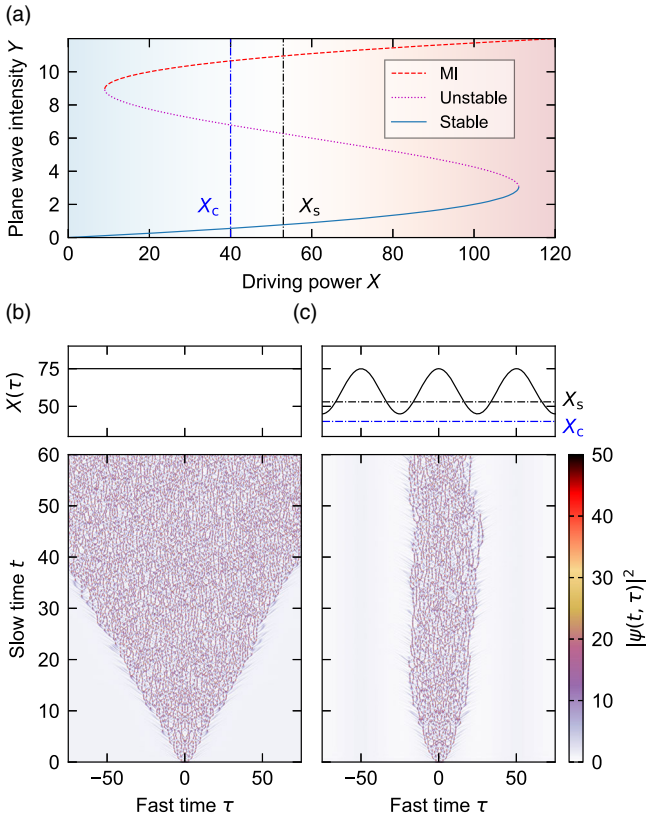

FIG. 1. (a) Intensity levels of the steady-state plane wave solutions of Eq. (1) for a detuning $\Delta = 9$ as a function of the driving intensity X. (b) Results obtained by numerically integrating Eq. (1) with the split-step Fourier method with a homogeneous driving intensity $X = 75$. The initial condition corresponds to the low-level homogeneous state superimposed with a localized perturbation, and gives rise to a uniformly expanding domain due to MI. (c) Numerical simulation results, showing how the expansion of the MI-induced domain can be arrested by a modulated driving field ($X_0 = 60$, $\omega = 2\pi/50$, $\varepsilon = 0.25$). Top panels in (b) and (c) highlight the driving profile $X(\tau)$ while black and blue horizontal curves in (c) show $X_s = 53$ and $X_c = 40$ (values pertinent to $\Delta = 9$), respectively.

[Fig. 1(a)], with the upper branch exhibiting a Turing-type dissipative MI that can give rise to complex behaviour with chaotic spatiotemporal character [32,41]. Our numerical simulations of Eq. (1) show that such spatiotemporally chaotic behaviour persists only for driving intensities above a certain, detuning-dependent threshold ($X > X_s$). For driving intensities below the threshold ($X < X_s$), the spatiotemporally chaotic state exists only as a transient; it decays entirely to the homogeneous state for intermediate values ($X_c < X < X_s$) while persisting localized structures known as Kerr cavity solitons [22,31,42–49] can emerge for lower values ($X < X_c$) (see Supplemental Material [50]).

For $X > X_s$, the stable plane wave state and the spatiotemporally chaotic state that emerges from MI can both exist in quasi-steady-state. However, the former is found to exhibit metastability at the expense of the latter [30,31]: a sufficiently strong localized perturbation that switches the stable plane wave state to the modulationally unstable upper state results in the nucleation of an expanding domain of spatiotemporal complexity [see Fig. 1(b)]. Thanks to the bistability, the modulationally *stable* plane wave background that surrounds the domain will not undergo MI even in the presence of broadband noise; the domain walls (fronts) that segregate the different states move with quasi-uniform velocity until the spatiotemporally chaotic state fills the entire system [31,32,53]. (See Supplemental Material [50] for a discussion on the front velocity.)

To arrest the front motion—and hence realise persisting localization—we leverage the fact that the spatiotemporally chaotic state decays to the stable plane wave background for $X < X_s$. Specifically, we apply a periodic modulation atop the cavity driving field,

$$X \to X(\tau) = X_0[1 + \varepsilon \cos(\omega\tau)], \tag{2}$$

where X_0 is the average intensity of the drive, and ε and ω are the depth and frequency of the modulation, respectively. By choosing ε and ω such that $X(\tau) < X_s$ across a sufficient interval around the minima of the drive, the spatiotemporally chaotic state born from MI is forced to remain confined in the vicinity of the maximum of the drive, where it is locally induced [see Fig. 1(c) and Supplemental Material [50]]. The modulation effectively prohibits the expansion of the domain due to the decay of perturbations entering the $X(\tau) < X_s$ region. We must emphasize that these dynamics occur despite the fact that the driving field exceeds at all τ the absolute threshold of MI: it is the bistability and the nonlinear dynamics of the system that permit the localization of MI. We also note that the dynamics of the confinement appear different from the usual dynamics that underpin localization in large classes of configurations, where (internal or external) modulations pin the fronts that segregate the two states by unfolding the system's Maxwell point [34,53–57]; here, in contrast, our simulations suggest that the localization can be interpreted in terms of the instability

of the spatiotemporally chaotic state in the $X(\tau) < X_s$ region (see also Supplemental Material [50]).

For experimental demonstration, we use a dispersive Kerr resonator constructed from an 85-m-long segment of standard single-mode optical fiber (SMF-28) that is looped on itself with a 95:5 coupler [see Fig. 2(a) and Supplemental Material [50]]. The resonator additionally includes a 99:1 coupler through which the intracavity dynamics are monitored. It has an overall finesse of about 40, corresponding to 60 kHz resonance width. We coherently drive the resonator with a train of flat-top, 6.5-ns-long pulses, obtained by amplitude modulating a continuous wave (cw) distributed feedback fiber laser at 1550 nm with the help of a signal derived from a pulse pattern generator [PPG 1 in Fig. 2(a)]. The PPG is referenced to an external clock with frequencies between 1 and 3 GHz, and we carefully adjust the clock frequency so as to synchronize the repetition rate of the driving pulse train with the 420-ns round-trip time of the resonator. (Small residual desynchronizaton is unlikely to significantly affect the dynamics.) Using this same clock signal, we are able to synchronously imprint sinusoidal modulation atop the nanosecond pulses with variable modulation depth ε and frequency ω. The modulated nanosecond pulses are finally amplified to about 5.7 W (average power level across a single pulse, corresponding to $X_0 \approx 60$) before being launched into the cavity. At this point, we must emphasize that our system is fundamentally different from the recirculating fiber loop used, e.g., by Kraych *et al.* to study nonlinear stages of *conservative* MI [29]: our system is far-from equilibrium, its dynamics dominated by dissipative effects [coherent driving and losses as described by Eq. (1)], while the experiment of Kraych *et al.* essentially samples conservative dynamics described by the NLSE.

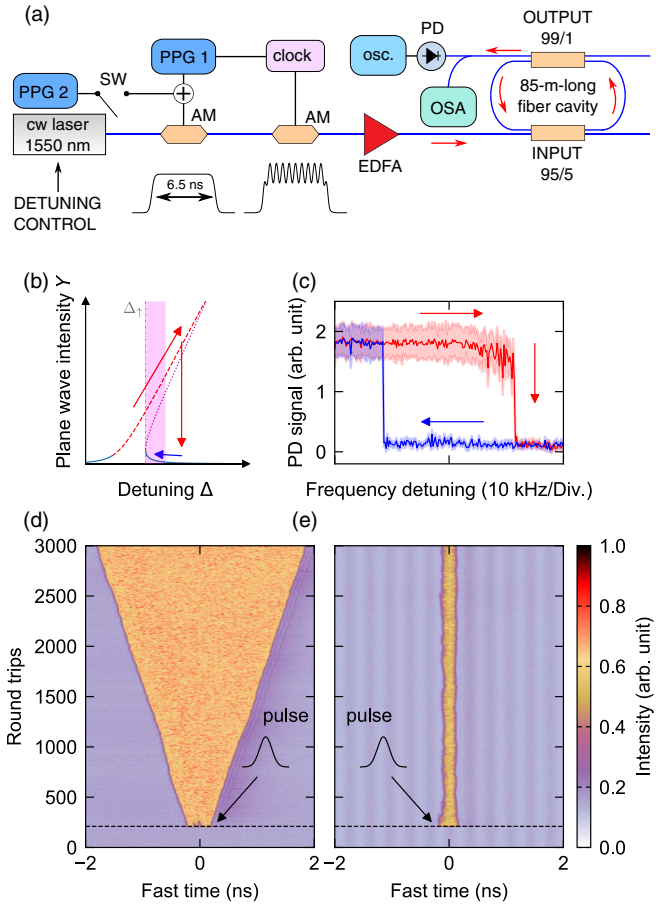

FIG. 2. (a) Schematic diagram of the experimental setup. Amplitude modulator (AM), Erbium-doped fibre amplifier (EDFA), oscilloscope (osc.), optical spectrum analyzer (OSA), photodetector (PD). (b) Illustration of a nonlinearly tilted cavity resonance. Stable plane wave state and persisting spatiotemporal chaos can coexist for detunings slightly above the beginning of plane wave bistability (magenta shaded region). (c) Experimental measurement of the hysteresis around the up-switching point. Solid curves show the mean intensity of the intracavity field as the pump-cavity detuning is increased (red curve) or decreased (blue curve). Shaded regions correspond to one-quarter of the standard deviation of the recorded intensity, highlighting the incoherent (coherent) character of the state born from MI (plane wave). (d),(e) Concatenation of oscilloscope traces, showing how a perturbation pulse permits the deterministic excitation of a localized domain. In (d) the driving field exhibits no modulation and the MI domain expands uniformly. In (e), a modulation with $\varepsilon = 0.25$ applied on the driving field arrests the expansion, localizing the spatiotemporal complexity.

To experimentally identify the regime where persistent MI-driven spatiotemporal chaos and stable plane wave states coexist, we leverage the underlying hysteresis behavior (Figs. 2(b) and 2(c); see also Ref. [32]). Specifically, for fixed driving intensity, the two states coexist over a narrow region of cavity detunings just above the up-switching point $\Delta_\uparrow$ that marks the beginning of plane wave bistability [Fig. 2(b)] [30,31]. We use the detuning control scheme introduced in Ref. [58] to first actively stabilize the detuning at a value $\Delta < \Delta_\uparrow$, where the chaotic state is the only state available. We then slowly increase the detuning lock point so as to identify the value at which that state falls down to the homogeneous state. By slightly reducing the detuning from this value, we are able to initialize the experiment on the low-level homogeneous state in the coexistence region [see Fig. 2(c)].

Once the system is prepared, we deterministically induce a localized domain that undergoes MI. This is achieved by using a second pulse pattern generator [PPG 2 in Fig. 2(a)] and an electronic switch [SW] to imprint a single perturbation pulse atop the modulated driving field. As in the simulations shown in Figs. 1(b) and 1(c), the perturbation locally switches the stable plane wave state to the modulationally unstable upper state, inducing MI.

Figure 2(d) shows experimentally measured dynamics when MI is induced in the absence of driving field modulation ($\varepsilon = 0$). The results shown were derived from a single long oscilloscope trace recorded at the 99:1

coupler of our cavity by dividing the trace into segments that approximately span one cavity round trip; Fig. 2(d) is the vertical concatenation of the resulting segments [59]. The addressing pulse is launched into the cavity around round trip 200, and gives rise to a spatiotemporally complex domain that expands quasilinearly. (Note that the ringing at the trailing edge of the data arises from the impulse response of the photodetector used.) We then repeat the experiment with the modulation depth set to $\varepsilon = 0.25$ and frequency $\omega = 2\pi \times 2.9$ GHz (corresponding to a modulation period of 350 ps). Results are shown in Fig. 2(e), evidencing the formation of a localized domain that remains confined within a single modulation cycle of the drive. Corresponding numerical simulations that use experimental parameters display similar behavior, and further reveal that the emergent localized state consists of chaotically fluctuating pulsations with picosecond durations (see Supplemental Material [50]).

Once excited, the localized domains can persist for several minutes (limited only by our ability to maintain system stability), corresponding to tens of millions of characteristic cavity photon lifetimes (or tens of gigameters of propagation distance). They can also be deterministically *erased* by applying a localized dip on the driving field at the position of the domain. Figures 3(a) and (b) show measured and simulated dynamics of such an erasure event, respectively, with $\varepsilon = 0.25$ and $\omega = 2\pi \times 2.7$ GHz. In contrast to excitation—which can be achieved by means of just a single addressing pulse—we have found that erasure generally requires the dip to be synchronously applied for several round trips across the entire domain. Note that the simulation results shown in Fig. 3(b) were obtained by numerically integrating the dimensional variant of Eq. (1) using parameters that correspond to our experiments; the raw simulation data was subsequently convolved with an 80 ps response function to mimic our experimental detection scheme (see Supplemental Material for raw simulation data [50]).

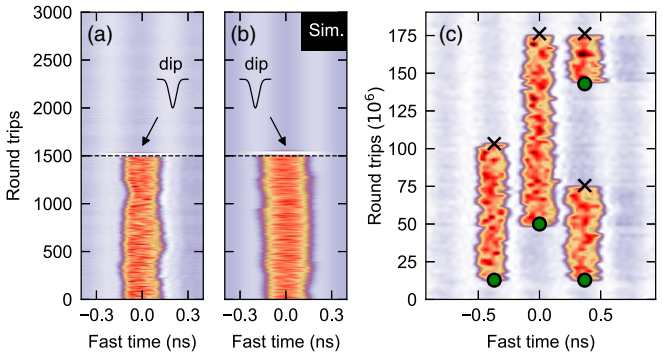

FIG. 3. (a) Experimental results, showing how a dip perturbation permits the deterministic erasure of a chaotic domain. (b) Numerical simulation results corresponding to the experiments shown in (a). The simulation results were obtained from integration of Eq. (1) and subsequently convolved with an 80 ps detector response function to facilitate comparison with our experiments. (c) Experimental demonstration of individual and parallel addressing of three localized MI domains. Solid green circles (black crosses) highlight roundtrips and locations where pulse (dip) perturbations are added on the driving field. Color bar for all panels is the same as in Figs. 2(d) and 2(e). Note the different axis limits in (a),(b), and (c).

The excitation and erasure processes can also be applied in parallel, allowing for the individual and simultaneous addressing of several spatiotemporally chaotic domains. Figure 3(c) shows experimentally measured dynamics when three domains—associated with three adjacent modulation cycles of the drive—are turned on and off. As can be seen, the addressing of one domain does not affect its neighbours. While similar individual addressing has been previously demonstrated for spatial [11] and temporal cavity solitons [13,60], the results shown in Fig. 3 represent—to the best of our knowledge—the first demonstrations of such addressing for spatiotemporally chaotic states born from MI.

In addition to individual addressing, the characteristics and dynamics of the localized domains can be controlled by manipulating the modulation applied on the driving field. On the one hand, adjustment of the frequency ω of the modulation naturally offers a straightforward route to control the size of the domain, as illustrated in Figs. 4(a)–4(c). Here we show experimentally observed localization for

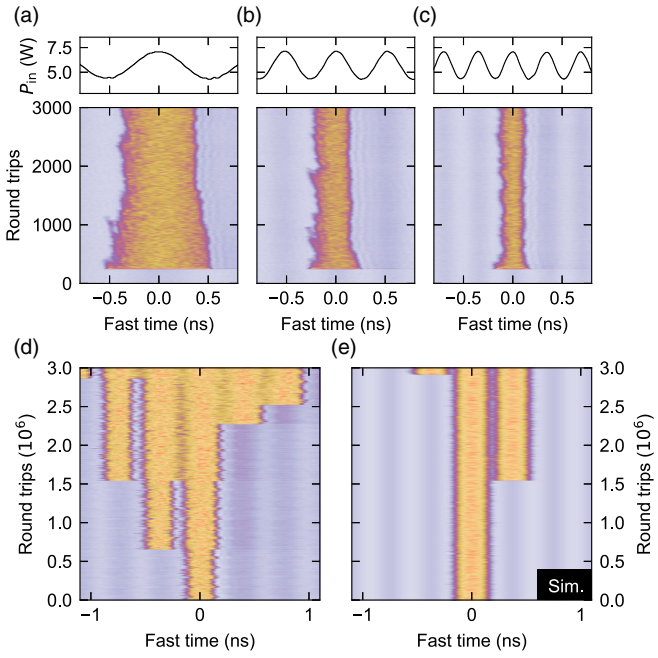

FIG. 4. (a)–(c), Experimental results, showing the emergence of localized domains born from MI for three different modulation frequencies applied on the driving field: (a), 0.96; (b), 1.9; (c), 2.9 GHz. For each case, the modulation depth $\varepsilon \approx 0.25$. The top panels show oscilloscope recordings of the driving field intensity profiles. (d) Experimentally observed discrete transport of domains, realized with an intermediate modulation depth $\varepsilon \approx 0.20$ and a modulation frequency of 2.7 GHz. (e) Numerical simulation results corresponding to experiments in (d). Color bar for all panels is the same as in Figs. 2(d) and 2(e).

three different modulation frequencies as indicated; for each case, the domain remains localized over a single modulation cycle of the drive (see also Supplemental Material on how the choice of ω can impact on the localization dynamics [50]). Adjustment of the modulation depth ε on the other hand allows to control the strength with which the fronts are pinned, and therefore the robustness of localization. As the modulation depth is increased from zero, we observe a crossover from quasi-linear expansion [Fig. 2(d)] to complete localization [Fig. 2(e)]. Interestingly, for intermediate modulation depths, our experiments reveal long-timescale discrete expansion, where the domains born from MI remain localized for extended periods but eventually undergo an abrupt expansion to fill the neighboring cycle of the modulated drive. Experimental results illustrating these dynamics are depicted in Fig. 4(d): we see that the initial, central domain remains localized for about 700 000 roundtrips (corresponding to more than 100 000 cavity photon lifetimes), yet eventually undergoes an abrupt expansion. Though experimental imperfections—such as pump-cavity desynchronization or pump inhomogeneities—can influence the specific features (e.g., give rise to additional asymmetries, see Ref. [56]), they do not appear to fundamentally underpin the dynamics; indeed, as illustrated in Fig. 4(e), similar behaviour is observed in our simulations of Eq. (1) that ignore all such imperfections. In loose analogy with quantum tunneling (or a particle with a deterministically fluctuating energy in a periodic potential), these observations suggest that there is a finite probability that a domain will become delocalized through discrete expansion, but with the probability per unit slow time decreasing near exponentially as the modulation depth increases (see also Supplemental Material [50]). We also note that the discrete expansion behavior can be considered a manifestation of pinning-depinning transitions that are central to front dynamics encountered in numerous nonequilibrium systems [53–56,61–64], here driven (predominantly) by deterministic fluctuations of the spatiotemporally chaotic state.

In summary, we have experimentally and numerically studied the nonlinear stages of dissipative modulation instability in a system with plane wave bistability—a coherently driven Kerr resonator. We have shown that the interplay between bistability, complex spatiotemporal dynamics, and inhomogeneous driving can give rise to persisting localized domains of MI-driven spatiotemporal chaos that can be turned on and off at will. It is worth noting that, while in our work the localization is achieved by modulating the driving field amplitude, similar dynamics should be possible by modulating the cavity detuning Δ [65] or the phase of the driving field [66].

It is interesting to speculate whether (and to what extent) the rich theoretical insights developed in the context of conservative NLSE systems [23–28] can be applied to elucidate the dynamics observed in our work. Moreover, we envisage that, by leveraging recent advances in ultrafast optical metrology [35,67], our system could allow for the monitoring of the picosecond-scale internal structure of the localized states in real time, thus permitting, e.g., experimental analyses of the states' Lyapunov exponents [32] and trajectories of the underlying attractors. We also note that the localized states observed in our system bear some resemblance to so-called chimeralike states [68–70]—spatiotemporal patterns characterized by the coexistence of coherent and incoherent domains in coupled systems—hinting at potential connections between the universal nonlinear phenomena of MI and chimeras. Finally, besides advancing our fundamental understanding of spatiotemporal complexity and MI, our system offers a route to generate customized patterns of noiselike pulses on demand [37,38], and could help elucidate instability dynamics that impact applications such as microresonator optical frequency combs [22,71].

We acknowledge financial support from The Royal Society of New Zealand in the form of Rutherford Discovery (RDF-15-UOA-015, for M. E.), James Cook (JCF-UOA1701, for S. C.) fellowships, as well as Marsden grants. M. G. C. acknowledges financial support from the Fondecyt 1210353 project. We also thank Miles Anderson for help in the initial stages of this project, as well as Gang Xu and Julien Fatome for help in the final stages of the work.

*Corresponding author.
m.erkintalo@auckland.ac.nz

[1] V. E. Zakharov and L. A. Ostrovsky, Modulation instability: The beginning, Physica (Amsterdam) **238D**, 540 (2009).
[2] T. B. Benjamin and J. E. Feir, The disintegration of wave trains on deep water Part 1. Theory, J. Fluid Mech. **27**, 417 (1967).
[3] T. Taniuti and H. Washimi, Self-Trapping and Instability of Hydromagnetic Waves Along the Magnetic Field in a Cold Plasma, Phys. Rev. Lett. **21**, 209 (1968).
[4] K. Tai, A. Hasegawa, and A. Tomita, Observation of Modulational Instability in Optical Fibers, Phys. Rev. Lett. **56**, 135 (1986).
[5] P. J. Everitt, M. A. Sooriyabandara, M. Guasoni, P. B. Wigley, C. H. Wei, G. D. McDonald, K. S. Hardman, P. Manju, J. D. Close, C. C. N. Kuhn, S. S. Szigeti, Y. S. Kivshar, and N. P. Robins, Observation of a modulational instability in Bose-Einstein condensates, Phys. Rev. A **96**, 041601 (2017).
[6] A. M. Turing, The chemical basis of morphogenesis, Phil. Trans. R. Soc. B **237**, 37 (1952).
[7] L. A. Lugiato and R. Lefever, Spatial Dissipative Structures in Passive Optical Systems, Phys. Rev. Lett. **58**, 2209 (1987).
[8] M. C. Cross and P. C. Hohenberg, Pattern formation outside of equilibrium, Rev. Mod. Phys. **65**, 851 (1993).
[9] N. Akhmediev and A. Ankiewicz, *Solitons: Nonlinear Pulses and Beams* (Chapman & Hall, London, 1997).

[10] D. Kip, M. Soljacic, M. Segev, E. Eugenieva, and D. N. Christodoulides, Modulation instability and pattern formation in spatially incoherent light beams, Science **290**, 495 (2000).
[11] S. Barland, J. R. Tredicce, M. Brambilla, L. A. Lugiato, S. Balle, M. Giudici, T. Maggipinto, L. Spinelli, G. Tissoni, T. Knödl, M. Miller, and R. Jäger, Cavity solitons as pixels in semiconductor microcavities, Nature (London) **419**, 699 (2002).
[12] Y. S. Kivshar and G. P. Agrawal, *Optical Solitons: From Fibers to Photonic Crystals*, 1st ed. (Academic Press, Amsterdam, Boston, 2003).
[13] F. Leo, S. Coen, P. Kockaert, S.-P. Gorza, P. Emplit, and M. Haelterman, Temporal cavity solitons in one-dimensional Kerr media as bits in an all-optical buffer, Nat. Photonics **4**, 471 (2010).
[14] D. R. Solli, C. Ropers, P. Koonath, and B. Jalali, Optical rogue waves, Nature (London) **450**, 1054 (2007).
[15] N. Akhmediev, A. Ankiewicz, and M. Taki, Waves that appear from nowhere and disappear without a trace, Phys. Lett. A **373**, 675 (2009).
[16] B. Kibler, J. Fatome, C. Finot, G. Millot, F. Dias, G. Genty, N. Akhmediev, and J. M. Dudley, The Peregrine soliton in nonlinear fibre optics, Nat. Phys. **6**, 790 (2010).
[17] J. M. Dudley, F. Dias, M. Erkintalo, and G. Genty, Instabilities, breathers and rogue waves in optics, Nat. Photonics **8**, 755 (2014).
[18] J. M. Dudley, G. Genty, A. Mussot, A. Chabchoub, and F. Dias, Rogue waves and analogies in optics and oceanography, Nat. Rev. Phys. **1**, 675 (2019).
[19] J. M. Dudley, G. Genty, and S. Coen, Supercontinuum generation in photonic crystal fiber, Rev. Mod. Phys. **78**, 1135 (2006).
[20] P. Del'Haye, A. Schliesser, O. Arcizet, T. Wilken, R. Holzwarth, and T. J. Kippenberg, Optical frequency comb generation from a monolithic microresonator, Nature (London) **450**, 1214 (2007).
[21] S. Coen and M. Erkintalo, Universal scaling laws of Kerr frequency combs, Opt. Lett. **38**, 1790 (2013).
[22] T. J. Kippenberg, A. L. Gaeta, M. Lipson, and M. L. Gorodetsky, Dissipative Kerr solitons in optical microresonators, Science **361**, eaan8083 (2018).
[23] V. E. Zakharov and A. A. Gelash, Nonlinear Stage of Modulation Instability, Phys. Rev. Lett. **111**, 054101 (2013).
[24] B. Kibler, A. Chabchoub, A. Gelash, N. Akhmediev, and V. E. Zakharov, Superregular Breathers in Optics and Hydrodynamics: Omnipresent Modulation Instability beyond Simple Periodicity, Phys. Rev. X **5**, 041026 (2015).
[25] G. Biondini and D. Mantzavinos, Universal Nature of the Nonlinear Stage of Modulational Instability, Phys. Rev. Lett. **116**, 043902 (2016).
[26] G. Biondini, S. Li, and D. Mantzavinos, Oscillation structure of localized perturbations in modulationally unstable media, Phys. Rev. E **94**, 060201(R) (2016).
[27] G. Biondini, S. Li, D. Mantzavinos, and S. Trillo, Universal Behavior of Modulationally Unstable Media, SIAM Rev. **60**, 888 (2018).
[28] M. Conforti, S. Li, G. Biondini, and S. Trillo, Automodulation versus breathers in the nonlinear stage of modulational instability, Opt. Lett. **43**, 5291 (2018).
[29] A. E. Kraych, P. Suret, G. El, and S. Randoux, Nonlinear Evolution of the Locally Induced Modulational Instability in Fiber Optics, Phys. Rev. Lett. **122**, 054101 (2019).
[30] F. Leo, L. Gelens, P. Emplit, M. Haelterman, and S. Coen, Dynamics of one-dimensional Kerr cavity solitons, Opt. Express **21**, 9180 (2013).
[31] M. Anderson, F. Leo, S. Coen, M. Erkintalo, and S. G. Murdoch, Observations of spatiotemporal instabilities of temporal cavity solitons, Optica **3**, 1071 (2016).
[32] Z. Liu, M. Ouali, S. Coulibaly, M. G. Clerc, M. Taki, and M. Tlidi, Characterization of spatiotemporal chaos in a Kerr optical frequency comb and in all fiber cavities, Opt. Lett. **42**, 1063 (2017).
[33] N. Verschueren, U. Bortolozzo, M. G. Clerc, and S. Residori, Spatiotemporal Chaotic Localized State in Liquid Crystal Light Valve Experiments with Optical Feedback, Phys. Rev. Lett. **110**, 104101 (2013).
[34] N. Verschueren, U. Bortolozzo, M. G. Clerc, and S. Residori, Chaoticon: Localized pattern with permanent dynamics, Phil. Trans. R. Soc. A **372**, 20140011 (2014).
[35] F. Bessin, F. Copie, M. Conforti, A. Kudlinski, A. Mussot, and S. Trillo, Real-Time Characterization of Period-Doubling Dynamics in Uniform and Dispersion Oscillating Fiber Ring Cavities, Phys. Rev. X **9**, 041030 (2019).
[36] M. Haelterman, S. Trillo, and S. Wabnitz, Dissipative modulation instability in a nonlinear dispersive ring cavity, Opt. Commun. **91**, 401 (1992).
[37] M. Horowitz, Y. Barad, and Y. Silberberg, Noiselike pulses with a broadband spectrum generated from an erbium-doped fiber laser, Opt. Lett. **22**, 799 (1997).
[38] C. Kerse, H. Kalaycıoğlu, P. Elahi, B. Çetin, D. K. Kesim, Ö. Akçaalan, S. Yavaş, M. D. Aşık, B. Öktem, H. Hoogland, R. Holzwarth, and F. Ö. Ilday, Ablation-cooled material removal with ultrafast bursts of pulses, Nature (London) **537**, 84 (2016).
[39] Y. K. Chembo and C. R. Menyuk, Spatiotemporal Lugiato-Lefever formalism for Kerr-comb generation in whispering-gallery-mode resonators, Phys. Rev. A **87**, 053852 (2013).
[40] *Dissipative Solitons*, Lecture Notes in Physics, edited by N. Akhmediev and A. Ankiewicz (Springer-Verlag, Berlin, Heidelberg, 2005).
[41] S. Coulibaly, M. Taki, A. Bendahmane, G. Millot, B. Kibler, and M. G. Clerc, Turbulence-Induced Rogue Waves in Kerr Resonators, Phys. Rev. X **9**, 011054 (2019).
[42] D. C. Cole, E. S. Lamb, P. Del'Haye, S. A. Diddams, and S. B. Papp, Soliton crystals in Kerr resonators, Nat. Photonics **11**, 671 (2017).
[43] W. Weng, R. Bouchand, E. Lucas, E. Obrzud, T. Herr, and T. J. Kippenberg, Heteronuclear soliton molecules in optical microresonators, Nat. Commun. **11**, 2402 (2020).
[44] H. Wang, Y.-K. Lu, L. Wu, D. Y. Oh, B. Shen, S. H. Lee, and K. Vahala, Dirac solitons in optical microresonators, Light Sci. Appl. **9**, 205 (2020).
[45] T. Herr, V. Brasch, J. D. Jost, C. Y. Wang, N. M. Kondratiev, M. L. Gorodetsky, and T. J. Kippenberg, Temporal solitons in optical microresonators, Nat. Photonics **8**, 145 (2014).
[46] P. Marin-Palomo, J. N. Kemal, M. Karpov, A. Kordts, J. Pfeifle, M. H. P. Pfeiffer, P. Trocha, S. Wolf, V. Brasch, M. H. Anderson, R. Rosenberger, K. Vijayan, W. Freude, T. J. Kippenberg, and C. Koos, Microresonator-based

solitons for massively parallel coherent optical communications, Nature (London) **546**, 274 (2017).
[47] P. Trocha, M. Karpov, D. Ganin, M. H. P. Pfeiffer, A. Kordts, S. Wolf, J. Krockenberger, P. Marin-Palomo, C. Weimann, S. Randel, W. Freude, T. J. Kippenberg, and C. Koos, Ultrafast optical ranging using microresonator soliton frequency combs, Science **359**, 887 (2018).
[48] M.-G. Suh and K. J. Vahala, Soliton microcomb range measurement, Science **359**, 884 (2018).
[49] J. Riemensberger, A. Lukashchuk, M. Karpov, W. Weng, E. Lucas, J. Liu, and T. J. Kippenberg, Massively parallel coherent laser ranging using a soliton microcomb, Nature (London) **581**, 164 (2020).
[50] See Supplemental Material at http://link.aps.org/supplemental/10.1103/PhysRevLett.127.123901 for additional experimental and theoretical details, which includes Refs. [51,52].
[51] G. A. El', A. V. Gurevich, V. V. Khodorovskii, and A. L. Krylov, Modulational instability and formation of a nonlinear oscillatory structure in a "focusing" medium, Phys. Lett. A **177**, 357 (1993).
[52] T. Tél and Y.-C. Lai, Chaotic transients in spatially extended systems, Phys. Rep. **460**, 245 (2008).
[53] Y. Pomeau, Front motion, metastability and subcritical bifurcations in hydrodynamics, Physica (Amsterdam) **23D**, 3 (1986).
[54] P. Coullet, C. Riera, and C. Tresser, Stable Static Localized Structures in One Dimension, Phys. Rev. Lett. **84**, 3069 (2000).
[55] F. Marino, G. Giacomelli, and S. Barland, Front Pinning and Localized States Analogues in Long-Delayed Bistable Systems, Phys. Rev. Lett. **112**, 103901 (2014).
[56] F. Marino, G. Giacomelli, and S. Barland, Splitting in the pinning-depinning transition of fronts in long-delayed bistable systems, Phys. Rev. E **95**, 052204 (2017).
[57] B. Garbin, Y. Wang, S. G. Murdoch, G.-L. Oppo, S. Coen, and M. Erkintalo, Experimental and numerical investigations of switching wave dynamics in a normally dispersive fibre ring resonator, Eur. Phys. J. D **71**, 240 (2017).
[58] A. U. Nielsen, B. Garbin, S. Coen, S. G. Murdoch, and M. Erkintalo, Invited Article: Emission of intense resonant radiation by dispersion-managed Kerr cavity solitons, APL Photonics **3**, 120804 (2018).
[59] Because of the absence of a robust timing reference exactly at the cavity round trip time, the segmentation time was chosen such that the front expansion is symmetric.
[60] Y. Wang, B. Garbin, F. Leo, S. Coen, M. Erkintalo, and S. G. Murdoch, Addressing temporal Kerr cavity solitons with a single pulse of intensity modulation, Opt. Lett. **43**, 3192 (2018).
[61] M. G. Clerc, C. Fernández-Oto, and S. Coulibaly, Pinning-depinning transition of fronts between standing waves, Phys. Rev. E **87**, 012901 (2013).
[62] A. J. Alvarez-Socorro, M. G. Clerc, M. A. Ferré, and E. Knobloch, Front depinning by deterministic and stochastic fluctuations: A comparison, Phys. Rev. E **99**, 062226 (2019).
[63] F. Haudin, R. G. Elías, R. G. Rojas, U. Bortolozzo, M. G. Clerc, and S. Residori, Driven Front Propagation in 1D Spatially Periodic Media, Phys. Rev. Lett. **103**, 128003 (2009).
[64] F. Haudin, R. G. Elías, R. G. Rojas, U. Bortolozzo, M. G. Clerc, and S. Residori, Front dynamics and pinning-depinning phenomenon in spatially periodic media, Phys. Rev. E **81**, 056203 (2010).
[65] A. K. Tusnin, A. M. Tikan, and T. J. Kippenberg, Nonlinear states and dynamics in a synthetic frequency dimension, Phys. Rev. A **102**, 023518 (2020).
[66] J. K. Jang, M. Erkintalo, S. Coen, and S. G. Murdoch, Temporal tweezing of light through the trapping and manipulation of temporal cavity solitons, Nat. Commun. **6**, 7370 (2015).
[67] P. Ryczkowski, M. Närhi, C. Billet, J.-M. Merolla, G. Genty, and J. M. Dudley, Real-time full-field characterization of transient dissipative soliton dynamics in a mode-locked laser, Nat. Photonics **12**, 221 (2018).
[68] Y. Kuramoto and D. Battogtokh, Coexistence of coherence and incoherence in nonlocally coupled phase oscillators, Nonlinear Phenom. Complex Syst. **5**, 380 (2002), http://www.j-npcs.org/abstracts/vol2002/v5no4/v5no4p380.html.
[69] D. M. Abrams and S. H. Strogatz, Chimera States for Coupled Oscillators, Phys. Rev. Lett. **93**, 174102 (2004).
[70] M. G. Clerc, M. A. Ferré, S. Coulibaly, R. G. Rojas, and M. Tlidi, Chimera-like states in an array of coupled-waveguide resonators, Opt. Lett. **42**, 2906 (2017).
[71] M. Karpov, M. H. P. Pfeiffer, H. Guo, W. Weng, J. Liu, and T. J. Kippenberg, Dynamics of soliton crystals in optical microresonators, Nat. Phys. **15**, 1071 (2019).